

# On-chip microwave coherent source with in-situ control of the photon number distribution

P. Mastrovito<sup>1,2,\*</sup>, H.G. Ahmad<sup>1,2</sup>, M. Esposito<sup>2</sup>, D. Massarotti<sup>3,2</sup>, and F. Tafuri<sup>1,4</sup>

<sup>1</sup> *Dipartimento di Fisica “Ettore Pancini”, Università di Napoli “Federico II,” Monte S. Angelo, I-80126 Napoli, Italy*

<sup>2</sup> *CNR-SPIN Complesso di Monte S. Angelo, 80126 Napoli, Italy*

<sup>3</sup> *Dipartimento di Ingegneria Elettrica e delle Tecnologie dell’Informazione, Università degli Studi di Napoli Federico II, via Claudio, I-80125 Napoli, Italy*

<sup>4</sup> *CNR-Istituto Nazionale di Ottica (CNR-INO), Largo Enrico Fermi 6, 50125 Florence, Italy*

(Dated: July 1, 2024)

Coherent photon sources are key elements in different applications, ranging from quantum sensing to quantum computing. In the context of circuit quantum electrodynamics, there have been multiple proposals for potential coherent sources of photons, but a well established candidate is still missing. The possibility of designing and engineering superconducting circuits behaving like artificial atoms supports the realization of quantum optics protocols, including microwave photons generation. Here we propose and theoretically investigate a new design that allows a tunable photon injection directly on-chip. The scheme is based on initiating a population inversion in a superconducting circuit that will act as the photon source of one or multiple target resonators. The key novelty of the proposed layout consists in replacing the usual capacitive link between the source and the target cavity with a tunable coupler, with the advantage of having on-demand control on the injected steady-state photons. We validate the dynamical control of the generated coherent states under the effect of an external flux threading the tunable coupler and discuss the possibility of employing this scheme also in the context of multiple bosonic reservoirs.

## I. INTRODUCTION

Precise control of photon population in bosonic elements, such as superconducting cavities, holds significant importance from both fundamental and practical perspectives in the realm of quantum sensing and computing. [1–8]. In this framework, a coherent photon source represents a key element to control the photon distribution in bosonic infrastructures [9–12]. Photon generation within the optical spectrum can be realized through multiple methods involving atoms, quantum dots, and nonlinear crystals [13–16]. In the context of Circuit Quantum ElectroDynamics (cQED), the majority of approaches take advantage of the atom-like nature of superconducting circuits and the strong dipole interaction between different elements [17–19]. The conventional approach to drive superconducting cavities is to have a capacitive connection to room temperature sources delivering microwave radiations, that generate specific coherent states depending on the quadrature components of the microwave pulse [9]. In this work, we present an alternative and versatile approach for generating a photon distribution

with a distinct average number of steady-state photons directly in situ with an inherently coherent photon source. Our proposal is based on engineering the spectrum and the transition rates of an artificial Josephson atom, which is a practice that has been extensively studied in different cQED platforms [20–24]. In particular, we consider an artificial atom able to work under the masing regime. In this hypothesis, the artificial atom operates as a natural on-chip micromaser able to emit microwave photons coherently [25–30]. When the artificial atom is coupled to a resonant cavity, serving as a reservoir, it generates a well defined number of steady-state photons within the cavity. The generated photon distribution depends on the transition rates between the energy levels protagonist of the masing dynamics, the loss rate in the target reservoir and the coupling between the photon source and the reservoir cavity [31]. Here we introduce a novel scheme for manipulating the coherent state generated within the target cavity. Instead of utilizing a fixed capacitive coupling between the photon source and the target cavity, we propose a tunable coupler scheme [32, 33]. This approach introduces tunability on the effective coupling strength that governs the interaction between the photon source and the target cavity, enabling precise control over the average number of injected photons. Moreover, assuming that the transition fre-

---

\* pasquale.mastrovito@unina.it

quency of the photon source can also be tuned while maintaining the transition rates unaltered, we can extend the fan-out of the system to multiple reservoirs resonating at different frequencies. This extension allows to individually manipulate different reservoirs according to the same dynamics of the single reservoir case. Photons demultiplexing can be employed in many fields, from quantum computing [34–36] to continuous variable encoding [37, 38].

## II. CONCEPT AND IMPLEMENTATION

A schematic of the setup for the implementation of the proposed system is shown in Fig. 1(a). The system consists of  $N_r + 2$  elements, where  $N_r$  represents the number of bosonic reservoirs on the output. The latter have resonance frequencies equal to  $\omega_{r_i}$ , where  $i$  ranges from 1 to  $N_r$  and  $\omega_{r_i} \neq \omega_{r_j}$  for any  $i \neq j$ . The remaining two elements correspond to the tunable photon source and the tunable coupler, each modeled for simplicity as two-level systems with transition frequencies  $\omega_s$  and  $\omega_c$ , that depend on the fluxes  $\Phi_s$  and  $\Phi_c$  respectively. By adequately engineering the system, the tunable coupler can be decoupled from the other elements, recreating an analog system of  $N_r + 1$  elements. In this hypothesis, the effect of the coupler is to renormalize the characteristic frequencies and coupling rates of the system by an amount that depends on its frequency. The ability to flux-tune the resonance frequency of the coupler defines a dynamical knob that gives control over the interaction between the photon source and a specific target reservoir, as depicted in Fig. 1(b). In the following section, we review the physics underlying the masing regime, on which the scheme is built upon. Subsequently, we discuss the methodology to effectively engineer the proposed scheme in the case of a single target resonator. We outline the key ingredients to build an experimentally feasible system that enables precise control over the photon population in the resonator via an external flux controlling the frequency of the tunable coupler. In this framework, we discuss different strategies to prevent detrimental effects coming from flux noise and faulty fabrication processes. We asses all these properties through a study of the second-order correlation function denoted as  $g^{(2)}(0)$ , which we use as an indicator of the emission performance of the photon source. We conclude the analysis of this scheme by simulating its behavior and discussing the extension to a scheme with multiple reservoirs, focusing on the capability to control each reservoir while avoiding cross-population individually.

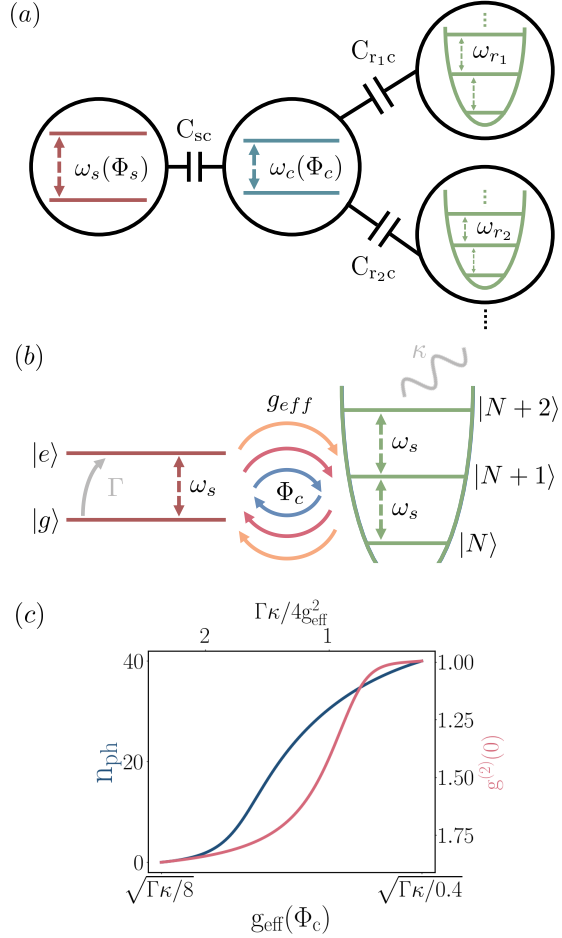


**FIG. 1:** (a) Sketch of the general setup with the corresponding spectral characteristics of each element. The first element from the left is the photon source. We ignore the higher energy levels required for population inversion and consider only the tunable transition energy  $\hbar\omega_s(\Phi_s)$  that is set on resonance with the target reservoir. The middle element is the tunable coupler with energy  $\hbar\omega_c(\Phi_c)$ , capacitively linked to various reservoirs with capacity  $C_{r_i c}$   $i = 1 \dots N_r$  and to the photon source with a capacitive coupling  $C_{sc}$ . (b) Depiction of the dynamics underlying photon injection. A counter-relaxation process represents population inversion in the system at a rate  $\Gamma$  from the ground state  $|g\rangle$  to the excited state  $|e\rangle$  of the system. The photon source is resonant with the cavity to populate it with several photons depending on the external flux  $\Phi_c$ . (c) The average number of steady-state photons  $n_{ph}$  and the second-order correlation function  $g^{(2)}(0)$  in terms of the effective coupling strength  $g_{eff}$  between the photon source and the cavity and in terms of the masing ratio  $\Gamma\kappa/4g_{eff}^2$  where  $\kappa$  is the loss rate of the reservoir.

### A. Masing regime

Before introducing the central idea of this work, we revisit the main notions related to the dynamics of an artificial atom operating within the masing regime, upon which our photon control and generation scheme is built. Masing is a physical phenomenon that governs the dynamics of masers and occurs when stimulated emissions prevail over absorption processes. Traditional masers typically involve multiple atoms and operate within a regime characterized by weak coupling [39]. However, in the realm of cQED, the strong coupling achievable between an artificial Josephson atom and photons permits the observation of the masing regime even at the level of a single artificial atom. In recent years there have been multiple demonstrations of single atom masing in cQED, employing a variety of techniques [40–43]. Some of these techniques are based on triggering population inversion directly on the single Josephson artificial atom [20, 26, 44–46], while others achieve it through hidden population inversion in dressed state systems [28, 30, 47]. All these approaches share a common requirement for observing the masing process: the transition frequency related to photon emission must be set on resonance with the frequency of the reservoir. To model the dynamics of a typical masing system, we adopt the treatment followed in Ref. [31]. We consider a reservoir characterized by a loss rate  $\kappa$ , which is capacitively coupled to an artificial atom. These two systems engage in resonant interaction via the transition frequencies characterized by population inversion in the artificial atom spectra. In the dynamics of the system, the condition of population inversion is represented by a counter relaxation rate  $\Gamma$ , which governs the driven transition from the low energy state  $|g\rangle$  to the high energy state  $|e\rangle$ . By considering just the emitting transition to model the artificial atom coupled to the reservoir, the system dynamics is well described by the Jaynes-Cummings Hamiltonian [48]:

$$\hat{H}_{JC} = \hbar\omega_r \hat{a}^\dagger \hat{a} + \frac{\hbar\omega_s}{2} \hat{\sigma}_z + \hbar g_{\text{eff}} (\hat{a}^\dagger \hat{\sigma}_- + \hat{a} \hat{\sigma}_+). \quad (1)$$

where  $\hat{a}^\dagger$  and  $\hat{a}$  are the creation and annihilation operators for the cavity mode,  $\hat{\sigma}_z$  is the Pauli-Z operator,  $\hat{\sigma}_-$  and  $\hat{\sigma}_+$  are the lowering and raising operators for the artificial atom,  $\omega_r$  is the cavity frequency,  $\omega_s$  is the artificial atom transition frequency, and  $g_{\text{eff}}$  represents the coupling strength between the atom and the cavity. The resonant coupling establishes

a photon-mediated interaction between the states  $|N, e\rangle \leftrightarrow |N+1, g\rangle$ . Here,  $|N, g\rangle$  ( $|N, e\rangle$ ) represents the system when the resonator is populated by  $N$  photons and the artificial atom is in the ground (excited) state. Assuming that the counter-relaxation process in the artificial atom transition is characterized by a rate  $\Gamma \gg g_{\text{eff}}$ , the dominant transition becomes  $|N, e\rangle \rightarrow |N+1, g\rangle$ . This predominance is directly linked to the counter-relaxation rate overcoming the atom-cavity coupling strength, which makes the artificial atom consistently appear in the excited state from the reservoir perspective during the typical interaction time ( $\sim 2\pi/g_{\text{eff}}$ ). Consequently, we can assume that the artificial atom is initially in the excited state. In this hypothesis, if the cavity contains  $N$  photons, the atom-cavity coupling  $g_{\text{eff}}\sqrt{N+1}$  induces dynamic transitions between the states  $|N, e\rangle$  and  $|N+1, g\rangle$ . Since  $\Gamma \gg g_{\text{eff}}$ , the transition will take the form of an incoherent process where any population that starts to accumulate in the state  $|N, g\rangle$  will quickly relax to the state  $|N, e\rangle$ . These two steps complete the transition from the state  $|N, e\rangle$  to the state  $|N+1, e\rangle$ , which allows to populate the cavity. This process will inevitably stop when the coupling strength  $g_{\text{eff}}\sqrt{N}$  becomes comparable or larger than the counter relaxation rate  $\Gamma$ . In this last situation the transition between  $|N, e\rangle$  and  $|N+1, g\rangle$  corresponds to the typical coherent oscillations of dressed state systems. The scaling of the Fock state ladder can also be limited by other two phenomena: photon blockade [49, 50] and the quantum Zeno effect [51, 52]. The photon blockade effect primarily arises from the proportional relationship between the splitting of the transition energy levels  $\Delta$  and the number of photons in the cavity ( $\Delta \propto \sqrt{N}$ ). As the number of injected photons increases, the resonant transition progressively deviates from the resonance condition. It is worth noting that a technique proposed in [50], involving an auxiliary cavity linked to the artificial atom, can mitigate the photon blockade effect. Hence, we will not consider this effect in our subsequent analysis. The quantum Zeno effect, instead, occurs for large values of  $\Gamma$  and results from the decoherence associated with the pumping process, which affects the quantum behavior of the system and, in turn, the masing regime [31, 52]. Considering a system where these last two phenomena can be neglected, we study the condition in which the masing regime takes place. Following the model used above for describing the dynamics under the masing regime, we can define the loss rate from the cavity to be  $\Gamma_l = N\kappa$ , while the emission rate linked to the atom-cavity transition will be  $\Gamma_e = 4Ng_{\text{eff}}^2/\Gamma$  [31]. Connecting these

rates, the emissions overcome the losses when the following condition is satisfied [31]:

$$\frac{\Gamma_l}{\Gamma_e} = \frac{\Gamma\kappa}{4g_{\text{eff}}^2} < 1. \quad (2)$$

Under this condition the interaction between the artificial atom and the cavity leads to photon population of the cavity through the mechanism described before, allowing the observation of the masing regime. Moreover, using a mean-field approximation, it is possible to also extract an analytical expression of the average number of steady-state photons that can be stored in the cavity [31]:

$$n_{\text{ph}} = \frac{\Gamma}{2\kappa} \left( 1 - \frac{\Gamma\kappa}{4g_{\text{eff}}^2} \right). \quad (3)$$

Eq. 3 shows that a system characterized by well-defined values of  $\Gamma$  and  $\kappa$  can attain a maximum number of photons, determined by the ratio  $\Gamma/2\kappa$ , when the masing ratio is far from unity ( $\Gamma\kappa/4g_{\text{eff}}^2 \ll 1$ ).

### B. Cavity control through tunable coupling

The model described above reveals that the cavity population is strongly dependent on the specific choices of the parameters  $\Gamma$ ,  $\kappa$ , and  $g$  in a masing system. Consequently, the tunability of one of these parameters enables a complete control of the steady-state photon population in the target cavity, within a range that depends on the tunability of one or more of these parameters and on the others. In this study, we explore the implementation of a tunable coupler scheme [32] to manipulate the coupling strength  $g$  between the photon source and a target reservoir. The proposed configuration, depicted in Fig. 1(a-b), comprises a two-level system coupled to a superconducting cavity through a flux-tunable qubit. We can effectively model the dynamics of this system by using a Hamiltonian that incorporates the free evolution terms of its constituent elements and the exchange interactions until the next nearest neighbors. Taking into account just the two levels in the photon source spectra forming the transition protagonist of the resonant interaction with the target

cavity, the Hamiltonian takes the following form:

$$\begin{aligned} \frac{\hat{H}}{\hbar} &= \hat{H}_s + \hat{H}_c + \hat{H}_r + \hat{H}_{rc} + \hat{H}_{sc} = \\ &\sum_{i=s,c} \frac{\omega_i \hat{\sigma}_i^z}{2} + \omega_s \hat{a}^\dagger \hat{a} + g_{rc} (\hat{a}^\dagger \hat{\sigma}_c^- + \hat{a} \hat{\sigma}_c^+) + \\ &+ g_{sc} (\hat{\sigma}_s^+ \hat{\sigma}_c^- + \hat{\sigma}_s^- \hat{\sigma}_r^+) + g_{sr} (\hat{\sigma}_s^+ \hat{\sigma}_c^- + \hat{\sigma}_s^- \hat{\sigma}_r^+). \end{aligned} \quad (4)$$

Here,  $\omega_j$ ,  $\hat{\sigma}_j^z$ ,  $\hat{\sigma}_j^+$ , and  $\hat{\sigma}_j^-$  for  $j = s, c$ , represent the transition frequency and the Z-Pauli, raising and lowering operators for the photon source and the tunable coupler, respectively. Additionally,  $\hat{a}$  and  $\hat{a}^\dagger$  are the ladder operators associated with the target resonator modes. The terms  $g_{ij}$  for  $i \neq j = s, r, c$  represent the coupling strengths governing the interactions between the different elements. Dynamic control over the coupling between the photon source and the cavity can be achieved by engineering a dispersive coupling with the tunable coupler for both the photon source and the cavity, where  $g_{jc} \ll \Delta_{jc} = \omega_j - \omega_c$  for  $j = s, r$ . Under this assumption, we can transform the Hamiltonian in Eq. 4 using a Schrieffer-Wolff transformation through the unitary operator  $\hat{U} = \exp \left[ \frac{g_{sc}}{\Delta_{sc}} (\sigma_s^+ \sigma_c^- - \sigma_s^- \sigma_c^+) + \frac{g_{rc}}{\Delta_{rc}} (\hat{a}^\dagger \sigma_c^- - \hat{a} \sigma_c^+) \right]$  that decouples the coupler from the other elements up to second order in  $g/\Delta$ . This transformation results in a Jaynes-Cummings Hamiltonian with a flux-tunable coupling strength (further details in the Appendix)

$$\frac{\hat{U} \hat{H} \hat{U}^\dagger}{\hbar} = \frac{\tilde{\omega}_s \hat{\sigma}_s^z}{2} + \tilde{\omega}_r \hat{a}^\dagger \hat{a} + g_{\text{eff}} (\hat{\sigma}_s^+ \hat{a} + \hat{\sigma}_s^- \hat{a}). \quad (5)$$

In this context, the influence of the capacitive couplings to the tunable coupler is quantitatively expressed by the renormalization of the characteristic frequencies governing the dynamics of the system. Specifically,  $\tilde{\omega}_k = \omega_k + \frac{g_{kc}^2}{\Delta_{kc}}$  with  $k = s, r$  represent the Lamb-shifted qubit and reservoir frequency, while  $g_{\text{eff}} = g_{sc} g_{rc} (1/\Delta_{sc} + 1/\Delta_{rc})$  characterizes the effective coupling between the photon source and the reservoir. The dependence on  $\omega_c$  embedded within  $\Delta_{sc}$  and  $\Delta_{rc}$  offers a knob to regulate the coupling strength  $g_{\text{eff}}$  between the source and the cavity through an external flux modulating the coupler frequency. The result is an intrinsically quantum photon source at cryogenic temperatures, enabling on-demand control of photon flow into a target cavity through an external flux threading the coupler. The key factors for the practical feasibility of this scheme are the selection of the initial working point and the robustness against unwanted flux

and design variations. The working point is determined by the choice of the counter-relaxation rate  $\Gamma$  and the loss rate of the target cavity  $\kappa$ . As highlighted in Eq. 3, the selection of these two parameters dictates whether the system can coherently inject photons into the target cavity and also determines the maximum number of steady-state photons that can be stored within the target cavity in the masing regime. The degree of tunability with the external flux  $\Phi_c$  over the steady-state photon distribution is evaluated by examining the second-order correlation function  $g^{(2)}(0) = \langle \hat{a}^\dagger \hat{a}^\dagger \hat{a} \hat{a} \rangle / \langle \hat{a}^\dagger \hat{a} \rangle^2$ . The latter is a commonly used metric for distinguishing quantum effects from classical phenomena in quantum optics systems [41]. In the context of this scheme, we use it as an indicator of the operational regime of the system [31], as illustrated in Fig. 1(c). When  $g^{(2)}(0) = 1$ , the system is in the masing regime, where the target cavity gets populated by  $\Gamma/2\kappa$  photons through its interaction with the photon source, while for  $g^{(2)}(0) = 2$  the system is in the thermal regime where the masing regime is suppressed and there is no effective population of the cavity. The suppression of the masing regime can occur when the coupling between the photon source and the cavity decreases to a point where the loss rate of photons equals or exceeds the photon injection rate into the cavity. To maximize the range of photon distributions that can be generated in the cavity, the system must be engineered in a way that allows to pass from the masing to the thermal regime within the available range of effective coupling. Considering a generic working point  $(\Gamma, \kappa)$  with an effective coupling that can be tuned inside a certain range of values, the more the system can span between  $g^{(2)}(0) = 1$  and  $g^{(2)}(0) = 2$ , the wider is the range of average steady-state photons that can be injected in the cavity. To quantitatively assess the working area of the system, we compute the second-order correlation function using the model in Eq. 5 with QuTip [53] and estimate the variation of  $g^{(2)}(0)$  within a certain range of effective coupling. Considering Eq. 3, we evaluate the variation of the second-order correlation function between the cases where  $g_{\text{eff}} = \sqrt{\Gamma\kappa}/8$  and  $g_{\text{eff}} = \sqrt{\Gamma\kappa}/0.4$  which, in good approximation, correspond to two situations where the cavity is maximally and minimally populated, respectively. The final results are depicted in Fig. 2, where the colormap highlights the expected variations of  $g^{(2)}(0)$  inside a range of experimentally reachable working points of the system [30, 50]. The red points in the colormap represent the maximum variation of  $\Delta g^{(2)}$  indicating the working points where the number of steady-state photons

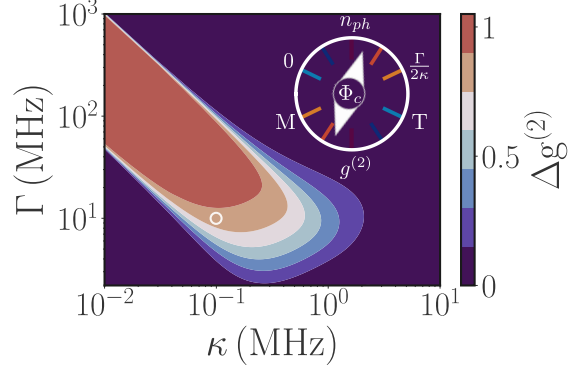


**FIG. 2:** Variation of the second-order correlation function  $g^{(2)}(0)$  as a function of the counter-relaxation rate  $\Gamma$  and the loss rate in the target cavity  $\kappa$ , while considering a range of coupling strengths from  $g_{\text{eff}} = \sqrt{\Gamma\kappa}/8$  to  $g_{\text{eff}} = \sqrt{\Gamma\kappa}/0.4$ . The white circle marks the working point used in this study for validating the photon source scheme. The role of the flux  $\Phi_c$  tuning the coupling  $g_{\text{eff}}$  in this point is figuratively represented as a flux-dependent knob, allowing the transition between deep Masing (M) and Thermal (T) regime. This control mechanism regulates consequently the average number of steady-state photons injected into the target reservoir.

injected into the cavity can span in the entire range from 0 to  $\Gamma/2\kappa$ . The dark blue area, conversely, contains the working points where there is no degree of control via the external flux in the considered range of effective coupling. Even when the system is well designed to operate in an appropriate working point, it must also possess robustness against fabrication errors, which can impact the position of the working point on the map, and against flux noise in the system, which can negatively affect the control over the steady-state photons distribution. To prevent the influence of faulty fabrication on the system feasibility, the coupling can be engineered to work within a broader range. This expansion of the coupling range, however, comes at the expense of an increased sensitivity of the tunable coupler to external flux. In a practical realization of the system, a trade-off must be found between these two features. To decrease the sensitivity to external flux, we can employ several strategies that allow to define the range of coupling of the system precisely. Differently from the typical tunable coupler scheme in which the system is engineered to have an off-point value where the coupling is canceled [32], here we just aim to modulate it within a specific range. One approach involves designing the tunable coupler with a resonance frequency lower than that of the photon source and the reservoir, resulting in an effec-

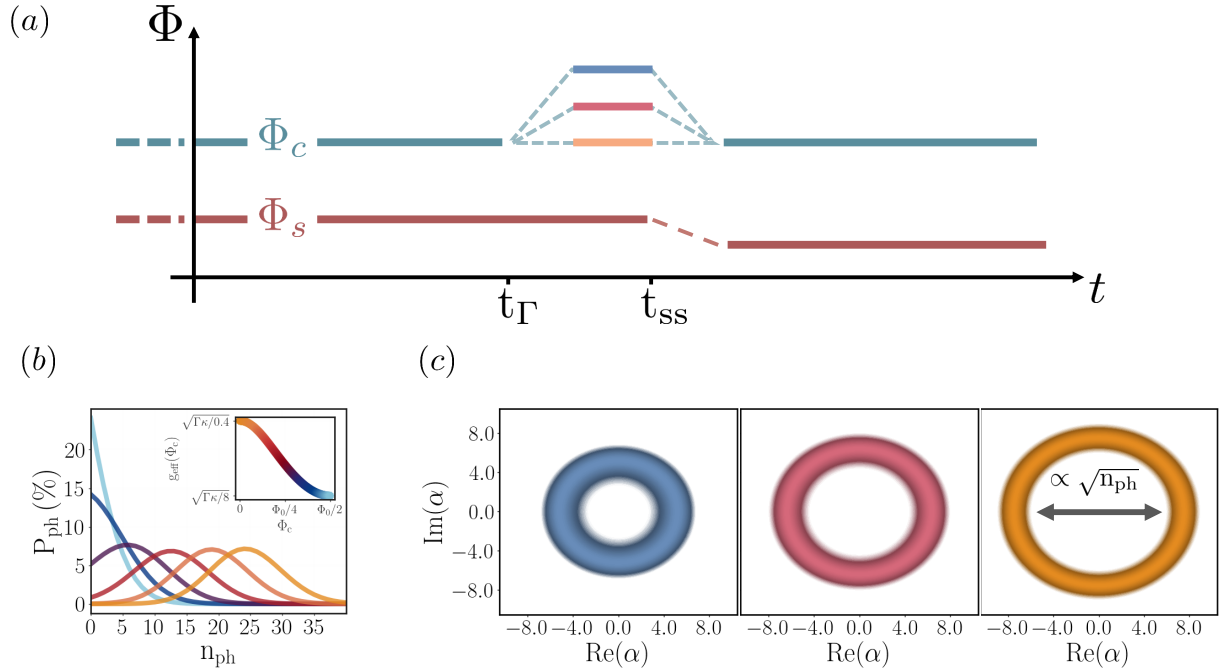


**FIG. 3:** Coherent photon generation through the tunable coupler scheme. (a) Flux timing diagram illustrating the photon population protocol of a single reservoir with the proposed scheme. At the initial time  $t_\Gamma$  the counter-relaxation is switched on. Afterwards the flux  $\Phi_c$  on the tunable coupler is chosen according to the wanted steady-state distribution of photons in the reservoir. After the time  $t_{ss}$  where the system has reached its steady state, the photon source is set off resonance from the reservoir to avoid further interactions between the two systems. (b) Steady-state photon distributions in the target reservoir under varying flux  $\Phi_c$  values threading the coupler. These simulation results are obtained for a device engineered according to the parameters listed at the end of paragraph IIB. Each color represents the distribution of photons in the Fock basis corresponding to specific values of the flux  $\Phi_c$ . (c) Steady-state reservoir normalized Wigner functions for different values of the flux  $\Phi_c$ . The radius of the Wigner function in the phase space is proportional to the average of the corresponding photon number distribution

tive coupling strength  $g_{\text{eff}} \propto 1/(\omega_s - \omega_c)$ . Additionally, we can use an asymmetric SQUID as the tunable element of the tunable coupler, which exhibits a more gradual response to external fluxes [54]. These adjustments provide two significant advantages: (1) the coupler never approaches a frequency close to those of the photon source and the reservoir for any threaded flux, ensuring that the dispersive condition is consistently met; (2) the asymmetry allows for non-zero minima in the coupler frequency, narrowing the range of effective coupling to well-defined maxima and minima. Alternative solutions rely on employing a pulsed approach [55]. To demonstrate the feasibility of the proposed scheme, we consider the following system: a flux-tunable photon source with a counter-relaxation rate  $\Gamma = 10$  MHz, self-capacity of  $C_s = 100$  fF, and a transition frequency  $\omega_s = 5$  GHz that is resonant with a reservoir having a resonance frequency  $\omega_r = \omega_s$ , self-capacity of

$C_r = 400$  fF, and loss rate  $\kappa = 0.1$  MHz. The two are connected through a tunable coupler corresponding to an asymmetric flux-tunable qubit with Josephson energies  $E_{J_1}^c = 31.4$  GHz,  $E_{J_2}^c = 37.7$  GHz, and capacitive energy  $E_C^c = 70$  MHz. The coupling capacities between the photon source and the reservoir with the tunable coupler are  $C_{sc} = C_{rc} = 1$  fF. A design with these parameters is perfectly feasible for state of the art nanofabrication process and the value of  $\Gamma$  is near the one used in other works [30, 50]. We analyze the system dynamics for various values of the flux  $\Phi_c$  threading the coupler. By activating the pumping process and exploring the system across different flux values, we obtain the results shown in Fig. 3(b). Different values of the flux threading the coupler yield distinct values of the effective coupling  $g_{\text{eff}}$ , which ultimately lead to different photon distributions within the reservoir at the steady state. The Wigner function defining the

steady state of the reservoir for different values of the effective coupling are shown in Fig. 3(c). We observe the typical "donut" shape that characterizes coherent photon sources, where the radius of the Wigner function is proportional to the average of the steady-state photon distribution. After the reservoir has reached its steady state, the pumping and the flux threading the tunable coupler can be switched off. At this stage, to avoid further interactions between the photon source and the reservoir we can change the transition frequency of the photon source through the external flux  $\Phi_s$ .

### C. Multiple resonator generalization

Another advantage offered by the proposed scheme is the ability to address multiple cavities by exploiting the tunability of the photon source. Under the same assumptions as the single-reservoir case, we can extend the analysis to an  $N_r$ -reservoir system. The system is described by a Hamiltonian that includes additional terms related to the self-energy of different reservoirs, the coupling of each reservoir to the tunable coupler, and the second nearest neighbor cross-couplings between each resonator. In this discussion, we consider the simple case of a two-reservoir setup as a starting point, where the case of  $N_r$  reservoirs will be a direct generalization (calculations of the general  $N_r$  case are provided in the Appendix). We investigate the ability to individually address each reservoir through the external fluxes, threading the tunable coupler and assuming that the photon source can be tuned on resonance with both resonators separately. Assuming that both the coupler and the photon source behave as perfect two-level systems and neglecting second-order interactions, the Hamiltonian is written as:

$$\hat{H}_N = \hat{H}_s + \hat{H}_c + \hat{H}_t + \hat{H}_i + \sum_{j=s,r_1,r_2} \hat{H}_{jc} + \hat{H}_{ti}. \quad (6)$$

To remove the terms related to the coupler from the Hamiltonian and establish a feasible and controllable scheme, the coupler must be engineered to satisfy the conditions  $g_{jc}/\Delta_{jc} \ll 1$  for  $j = s, r_1, r_2$ . Under this assumption, we can transform the Hamiltonian by applying the Schrieffer-Wolff transformation:

$$\hat{U} = \exp \left[ \frac{g_{sc}}{\Delta_{sc}} (\hat{\sigma}_s^+ \hat{\sigma}_c^- - \hat{\sigma}_s^- \hat{\sigma}_c^+) + \frac{g_{r_1c}}{\Delta_{r_1c}} (\hat{a}_{r_1}^\dagger \hat{\sigma}_c - \hat{a}_{r_1} \hat{\sigma}_c^\dagger) + \frac{g_{r_2c}}{\Delta_{r_2c}} (\hat{a}_{r_2}^\dagger \hat{\sigma}_c - \hat{a}_{r_2} \hat{\sigma}_c^\dagger) \right]. \quad (7)$$

This transformation leads to the following Hamiltonian:

$$\begin{aligned} \frac{\hat{H}}{\hbar} &= \frac{\tilde{\omega}_s \sigma_s^z}{2} + \tilde{\omega}_{r_1} a_{r_1} + \tilde{\omega}_{r_2} a_{r_2}^+ a_{r_2} \\ &+ \sum_{j=r_1,r_2} \tilde{g}_{jc} (\sigma_s^+ a_j + \sigma_s^- a_j^\dagger) \\ &+ \tilde{g}_{r_1 r_2} (a_{r_1} a_{r_2}^+ + a_{r_1}^+ a_{r_2}). \end{aligned} \quad (8)$$

In this expression, the renormalizations of various frequency terms are identical to those observed in the single-reservoir case, except for the new cross-coupling term  $\tilde{g}_{r_1 r_2}$  between the two reservoirs. The second-order coupling term  $g_{r_1 r_2}$  is summed with another term arising from the coupling between the reservoirs via the tunable coupler, leading to the following expression of the effective cross-coupling strength:

$$\tilde{g}_{r_1 r_2} = g_{r_1c} g_{r_2c} \left( \frac{1}{\Delta_{r_1c}} + \frac{1}{\Delta_{r_2c}} \right) + g_{r_1 r_2}. \quad (9)$$

It is, therefore, crucial to understand how much detuning is required between the different reservoirs at the fan-out of the system to avoid resonant interactions that lead to cross-population between the cavities. We consider a setup similar to the single-reservoir scheme analyzed in the previous section, with the addition of a second cavity at a frequency  $\omega_{r_2} = \omega_{r_1} + \Delta$  and linked to the tunable coupler with the same capacitive coupling used for the target cavity. We observe the system behavior for different values of  $\Delta$  while sweeping both the photon source and the coupler frequencies, simulating the effect of the external fluxes  $\Phi_s$  and  $\Phi_c$  individually threading the two elements, respectively. Assuming that both reservoirs have the same linewidth as the reservoir considered in the previous single reservoir case  $\kappa_1 = \kappa_2 = 0.1\text{MHz}$ . To avoid cross-population between the two reservoirs the detuning  $\Delta = \omega_{r_1} - \omega_{r_2}$  must be much higher than the spectral linewidth of the two reservoirs ( $\Delta \gg \kappa$ ). In this case, we chose a detuning of  $\Delta/2\pi \geq 5\text{MHz}$ , that allows to individually address and control the steady-state population of each resonator with the proposed scheme. In Fig. 4(a), we show the behavior of the system, where

by setting the photon source on resonance with one of the cavities, it is possible to control their population without populating also the other resonator. For small detuning, the effective coupling between the source and the cavity has approximately the same dependence on the flux, even for a fixed value of the capacitive coupling between the cavity and the tunable coupler. When engineering systems are characterized by high detuning between the different reservoirs on the output, the respective capacitive links to the tunable coupler must be adequately designed. To optimize the device, the couplings must be chosen to preserve the shape of  $g_{\text{eff}}(\Phi_c)$ , because the effective coupling depends on the resonance frequency of the target reservoir  $\omega_t$ . We thus need to take into account the variation of this frequency by changing the coupling between the central coupler and the cavity under consideration. We use the same setup employed before, taking a reference cavity, with a resonance frequency  $\omega_{r_1}$  and a capacity  $C_{r_1c}$  linking the cavity to the central coupler. We consider a second cavity with a detuned resonance frequency of  $\omega_{r_2} = \omega_{r_1} + \Delta$  and with a coupling capacitor  $C_{r_2c} = \alpha C_{r_1c}$ , as depicted in Fig. 1(a). We assume that the self-capacity of the cavity does not change with its resonance frequency. If there is a change it will result in an additional factor on the expression of the coupling strength that can be absorbed by the factor  $\alpha$ , allowing the same type of analysis. Through a sweep on  $\Delta$  and  $\alpha$ , we study how the shape of  $g_{\text{eff}}(\Phi_c)$  changes by analyzing the Hausdorff distance relative to the reference curve obtained for the reference cavity. The results of this analysis are shown in Fig. 4(b), where we can clearly distinguish a blue region corresponding to the optimal values of the coupling capacity. For small values of the detuning  $\Delta$ , the ideal coupling correction  $\alpha$  is near unity and, in general, follows the shape  $\alpha = \sqrt{\omega_r/(\omega_r + \Delta)}$ .

### III. CONCLUSIONS

We have proposed a simple and versatile scheme for an on-demand coherent photon source on chip. The tunability inherent to this scheme enables precise control over the average of the steady-state photon distribution generated in a target reservoir while also facilitating the addressing of different cavities capacitively linked to the coupler, each characterized by distinct resonance frequencies. Initially, we consider the case of a single resonator, where after identifying a set of parameters for a practical design we have analyzed the system performance for var-

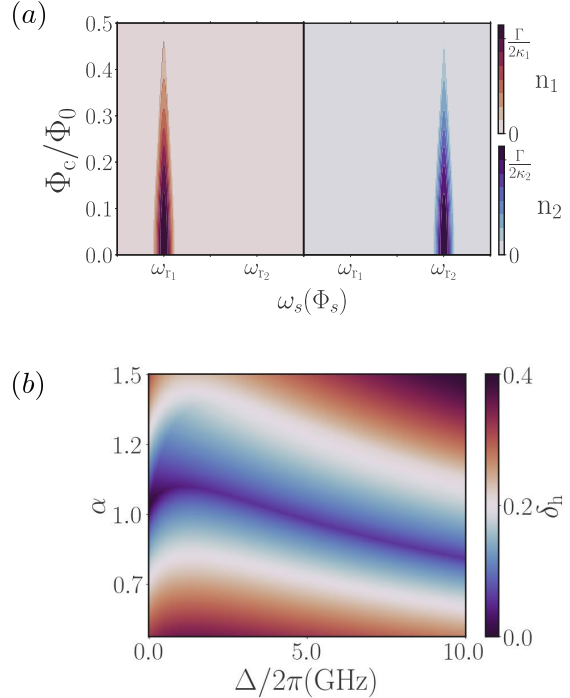


**FIG. 4:** Multiple reservoirs case photon population. (a) Steady-state photon number in different cavities with resonance frequencies  $\omega_{r_1}/2\pi = 5\text{GHz}$  and  $\omega_{r_2}/2\pi = 5.005\text{GHz}$ . The red and blue points on the two plots represent the average number of injected photons in each cavity for specific choices of flux  $\Phi_c$  and frequency  $\omega_s/2\pi$  of the photon source. The absence of colored points in correspondence to the frequency of the other resonator in each colorplot shows the absence of cross-population phenomena. The rest of the parameters are the same as the one considered in Fig. 3. (b) The Hausdorff distance between the effective coupling strength curve  $g_{\text{eff}}(\Phi_c)$  of the reference cavity and the second cavity detuned by  $\Delta$  and coupled with a coupling capacity  $\alpha$  times that of the reference cavity. The dark blue zone indicates a range of coupling capacities that maintain consistent effective coupling dependencies while altering the resonance frequency of the reservoir relative to the reference cavity.

ious fluxes applied across the coupler, demonstrating the capability of the proposed setup to control the photon distribution generated in a target cavity. Subsequently, we extend our analysis to a setup comprising an additional reservoir, showcasing the capability to individually address different reservoirs at different frequencies by adequately designing the detunings and the couplings in the system. The device acts as a tunable and finely controllable cryogenic micromaser, which can be an important tool in many



quantum architectures based on bosonic quantum systems, [34–36], like continuous variable quantum computing [37], quantum memories [56] and quantum metrology [57]. Moreover, the demultiplexing capability of the proposed scheme offers the advantage of decoupling multiple reservoirs from direct connections to room-temperature devices, leading to significant enhancements in terms of scalability. The scheme is also well-suited for 3D integrated systems, further expanding its domain of potential applications.

#### IV. ACKNOWLEDGMENTS

The authors thank F. Nori and A. Porzio for the fruitful discussion and would also like to thank G. Di Bello and M. Vizzuso for their help in the work development. The work was supported by the project “On-chip signal generation for superconducting quantum processors (SFQ4QPU)”, in the frame of Eurostars CoD 15 Call 2021, by the project “Superconducting quantum-classical linked computing systems (SuperLink)”, in the frame of QuantERA2 ERANET COFUND in Quantum Technologies, and by the Project PRIN 2022-Advanced Control and Readout of scalable Superconducting NISQ Architectures (SuperNISQ)-CUP E53D23001910006. The research activities were also supported by the PNRR MUR project PE0000023-NQSTI and the PNRR MUR project CN\_00000013—ICSC.

#### V. DATA AVAILABILITY

All the generated data supporting this study can be reproduced using the publicly available simulation codes.

#### VI. CODE AVAILABILITY

The source codes for the numerical simulations presented in the paper are available at <https://github.com/Pask97/on-chip-photon-source>

#### VII. APPENDIX

##### A. Hamiltonian

The photon source scheme in the most general case, with  $N$  resonators in output, can be described

by the following Hamiltonian:

$$\begin{aligned} \frac{\hat{H}_N}{\hbar} = & \hat{H}_s + \hat{H}_c + \hat{H}_{sc} \\ & + \sum_{n=1}^N (\hat{H}_{r_n c} + \hat{H}_{r_n} + \hat{H}_{sr_n}) \\ & + \sum_{n \neq m=1}^N \hat{H}_{r_n r_m}. \end{aligned} \quad (10)$$

Assuming that the coupler is in the transmon regime ( $E_J^c/E_J^c \geq 50$ ) and considering just the two level transitions on resonance with the reservoir for the photon source and the first transition level of the coupler, the hamiltonian terms can be rewritten as:

$$\hat{H}_{s,c} = \hbar \frac{\omega_{s,c} \sigma_{s,c}^z}{2}. \quad (11)$$

$$\hat{H}_{r_n} = \hbar \omega_r a_n^\dagger a_n. \quad (12)$$

$$\hat{H}_{r_n c} = \hbar g_{nc} (\hat{a}_n \hat{\sigma}_c^+ + \hat{a}_n^\dagger \hat{\sigma}_c^-). \quad (13)$$

$$\hat{H}_{sc} = \hbar g_{sc} (\hat{\sigma}_s \hat{\sigma}_c^+ + \hat{\sigma}_s \hat{\sigma}_c^-). \quad (14)$$

$$\hat{H}_{r_n r_m} = \hbar g_{nm} (\hat{a}_n \hat{a}_m^\dagger + \hat{a}_n^\dagger \hat{a}_m). \quad (15)$$

##### B. Schrieffer-Wolff transformation

To decouple the coupler from the other elements of the scheme we can use a Schrieffer-Wolff transformation. Before introducing the transformation for the general case we first consider the situation with a single reservoir. The case with a larger fan-out will be a simple generalization of the single reservoir case.

###### 1. Single reservoir

The Schrieffer-Wolff transformation that we used in the single reservoir case is:

$$\hat{U} = \exp \left[ \frac{g_{sc}}{\Delta_{sc}} (\hat{\sigma}_s^+ \hat{\sigma}_c^- - \hat{\sigma}_s^- \hat{\sigma}_c^+) + \frac{g_{rc}}{\Delta_{rc}} (\hat{a}^+ \hat{\sigma}_c^- - \hat{a} \hat{\sigma}_c^+) \right].$$

where  $\Delta_{sc} = \omega_s - \omega_c$  and  $\Delta_{rc} = \omega_r - \omega_c$  are respectively the detuning between the coupler with the main transition of the photon source and the reservoir. By applying this transformation on the single reservoir hamiltonian we pass from a three-body system to the following two-body system hamiltonian:

$$\frac{\hat{U} \hat{H}_1 \hat{U}^\dagger}{\hbar} = \tilde{\omega}_s \hat{\sigma}_s^z + \tilde{\omega}_r a^\dagger a + \tilde{g}_{sr} (\hat{a} \hat{\sigma}_c^+ + \hat{a}^+ \hat{\sigma}_c^-). \quad (16)$$

The characteristic frequencies of the system are renormalized:

$$\tilde{\omega}_s = \omega_s + g_{sc}^2 / \Delta_{sc}. \quad (17)$$

$$\tilde{\omega}_r = \omega_r + g_{rc}^2 / \Delta_{rc}. \quad (18)$$

$$\tilde{g}_{sr} = \omega_r + g_{rc}^2 / \Delta_{rc}. \quad (19)$$

For this calculation we have assumed that the coupler is always at the ground state.

## 2. Multiple reservoirs

To decouple the coupler from the source and the resonator on the fan-out of the scheme we can use a Schrieffer-Wolff transformation which is defined by the sum of various single resonator Schrieffer-Wolff transformation. We use the following unitary operator:

$$\hat{U} = \exp \left[ \frac{g_{sc}}{\Delta_{sc}} (\hat{\sigma}_s^+ \hat{\sigma}_c^- - \hat{\sigma}_s^- \hat{\sigma}_c^+) + \sum_{n=1}^N \frac{g_{nc}}{\Delta_{nc}} (\hat{a}_n^\dagger \hat{\sigma}_c^- - \hat{a}_n \hat{\sigma}_c^+) \right]. \quad (20)$$

By applying this transformation to the hamiltonian in Eq. 10 and keeping the terms up to the second order the hamiltonian is rewritten as follows:

$$\frac{\hat{U} \hat{H}_N \hat{U}^\dagger}{\hbar} = \frac{\tilde{\omega}_s \sigma_s^z}{2} + \sum_{n=1}^N [\tilde{\omega}_n \hat{a}_n^\dagger \hat{a}_n + \tilde{g}_{sn} (\hat{a}_n^\dagger \hat{\sigma}_s^- + \hat{a}_n \hat{\sigma}_s^+)] + \sum_{n \neq m}^N \tilde{g}_{nm} (a_n^\dagger a_m + a_n a_m^\dagger). \quad (21)$$

As before the effect of the coupler on the whole system is to renormalize the characteristic frequencies of the system as follows:

$$\tilde{\omega}_s = \omega_s + g_{sc}^2 / \Delta_s. \quad (22)$$

$$\tilde{\omega}_n = \omega_n + g_{nc}^2 / \Delta_n. \quad (23)$$

$$\tilde{g}_{sn} = \frac{g_{sc} g_{nc}}{2} \left( \frac{1}{\Delta_{nc}} + \frac{1}{\Delta_{sc}} \right) + g_{ns}. \quad (24)$$

$$\tilde{g}_{nm} = \frac{g_{nc} g_{mc}}{2} \left( \frac{1}{\Delta_{nc}} + \frac{1}{\Delta_{mc}} \right) + g_{nm}. \quad (25)$$

What we see is that the coupler also mediates the interaction between the various pairs of resonators but with respect to the interaction between the target reservoir and the photon source, it is an off resonance interaction that does not lead to any cross-population phenomena if the reservoir are adequately detuned between each other.

[1] S. Lloyd and S. L. Braunstein, Quantum computation over continuous variables, Physical Review

Letters **82**, 1784 (1999).

- [2] D. Gottesman, A. Kitaev, and J. Preskill, Encoding a qubit in an oscillator, *Physical Review A* **64**, 012310 (2001).
- [3] H. Goto, Universal quantum computation with a nonlinear oscillator network, *Physical Review A* **93**, 050301 (2016).
- [4] V. V. Albert, C. Shu, S. Krastanov, C. Shen, R.-B. Liu, Z.-B. Yang, R. J. Schoelkopf, M. Mirrahimi, M. H. Devoret, and L. Jiang, Holonomic quantum control with continuous variable systems, *Physical review letters* **116**, 140502 (2016).
- [5] R. W. Heeres, P. Reinhold, N. Ofek, L. Frunzio, L. Jiang, M. H. Devoret, and R. J. Schoelkopf, Implementing a universal gate set on a logical qubit encoded in an oscillator, *Nature communications* **8**, 94 (2017).
- [6] C. Liu, M. Mucci, X. Cao, M. V. G. Dutt, M. Hatridge, and D. Pekker, Proposal for a continuous wave laser with linewidth well below the standard quantum limit, *Nature Communications* **12**, 10.1038/s41467-021-25879-8 (2021).
- [7] Y. Lu, M. Kudra, T. Hillmann, J. Yang, H. Li, F. Quijandria, and P. Delsing, Resolving fock states near the kerr-free point of a superconducting resonator, *arXiv preprint arXiv:2210.09718* (2022).
- [8] A. Copetudo, C. Y. Fontaine, F. Valadares, and Y. Y. Gao, Shaping photons: Quantum information processing with bosonic cQED, *Applied Physics Letters* **124**, 080502 (2024).
- [9] M. Hofheinz, E. Weig, M. Ansmann, R. C. Bialczak, E. Lucero, M. Neeley, A. O'connell, H. Wang, J. M. Martinis, and A. Cleland, Generation of fock states in a superconducting quantum circuit, *Nature* **454**, 310 (2008).
- [10] M. Hofheinz, H. Wang, M. Ansmann, R. C. Bialczak, E. Lucero, M. Neeley, A. O'connell, D. Sank, J. Wenner, J. M. Martinis, *et al.*, Synthesizing arbitrary quantum states in a superconducting resonator, *Nature* **459**, 546 (2009).
- [11] S. Krastanov, V. V. Albert, C. Shen, C.-L. Zou, R. W. Heeres, B. Vlastakis, R. J. Schoelkopf, and L. Jiang, Universal control of an oscillator with dispersive coupling to a qubit, *Physical Review A* **92**, 040303 (2015).
- [12] W. Wang, L. Hu, Y. Xu, K. Liu, Y. Ma, S.-B. Zheng, R. Vijay, Y. Song, L.-M. Duan, and L. Sun, Converting quasiclassical states into arbitrary fock state superpositions in a superconducting circuit, *Physical Review Letters* **118**, 223604 (2017).
- [13] P. Senellart, G. Solomon, and A. White, High-performance semiconductor quantum-dot single-photon sources, *Nature nanotechnology* **12**, 1026 (2017).
- [14] A. S. Solntsev and A. A. Sukhorukov, Path-entangled photon sources on nonlinear chips, *Reviews in Physics* **2**, 19 (2017).
- [15] P. Thomas, L. Ruscio, O. Morin, and G. Rempe, Efficient generation of entangled multiphoton graph states from a single atom, *Nature* **608**, 677 (2022).
- [16] L. Di Palma, A. Miano, P. Mastrovito, D. Maszarotti, M. Arzeo, G. Pepe, F. Tafuri, and O. Mukhanov, Discriminating the phase of a coherent tone with a flux-switchable superconducting circuit, *Phys. Rev. Appl.* **19**, 064025 (2023).
- [17] A. A. Houck, D. Schuster, J. Gambetta, J. Schreier, B. Johnson, J. Chow, L. Frunzio, J. Majer, M. Devoret, S. Girvin, *et al.*, Generating single microwave photons in a circuit, *Nature* **449**, 328 (2007).
- [18] M. Pechal, L. Huthmacher, C. Eichler, S. Zeytinoglu, A. Abdumalikov Jr, S. Berger, A. Wallraff, and S. Filipp, Microwave-controlled generation of shaped single photons in circuit quantum electrodynamics, *Physical Review X* **4**, 041010 (2014).
- [19] Y. Li, Z. Wang, Z. Bao, Y. Wu, J. Wang, J. Yang, H. Xiong, Y. Song, H. Zhang, and L. Duan, Frequency-tunable microwave quantum light source based on superconducting quantum circuits, *arXiv preprint arXiv:2304.05847* (2023).
- [20] D. M. Berns, M. S. Rudner, S. O. Valenzuela, K. K. Berggren, W. D. Oliver, L. S. Levitov, and T. P. Orlando, Amplitude spectroscopy of a solid-state artificial atom, *Nature* **455**, 51 (2008).
- [21] K. Koshino, K. Inomata, T. Yamamoto, and Y. Nakamura, Implementation of an impedance-matched  $\lambda$  system by dressed-state engineering, *Physical review letters* **111**, 153601 (2013).
- [22] K. Inomata, K. Koshino, Z. Lin, W. Oliver, J. S. Tsai, Y. Nakamura, and T. Yamamoto, Microwave down-conversion with an impedance-matched  $\lambda$  system in driven circuit qed, *Physical review letters* **113**, 063604 (2014).
- [23] K. Inomata, Z. Lin, K. Koshino, W. D. Oliver, J.-S. Tsai, T. Yamamoto, and Y. Nakamura, Single microwave-photon detector using an artificial  $\lambda$ -type three-level system, *Nature communications* **7**, 12303 (2016).
- [24] Y.-H. Chang, D. Dubyna, W.-C. Chien, C.-H. Chen, C.-S. Wu, and W. Kuo, Circuit quantum electrodynamics with dressed states of a superconducting artificial atom, *Scientific Reports* **12**, 22308 (2022).
- [25] N. Hatakenaka and S. Kurihara, Josephson cascade micromaser, *Phys. Rev. A* **54**, 1729 (1996).
- [26] O. Astafiev, K. Inomata, A. Niskanen, T. Yamamoto, Y. A. Pashkin, Y. Nakamura, and J. Tsai, Single artificial-atom lasing, *Nature* **449**, 588 (2007).
- [27] S. André, P.-Q. Jin, V. Brosco, J. H. Cole, A. Romito, A. Shnirman, and G. Schön, Single-qubit lasing in the strong-coupling regime, *Phys. Rev. A* **82**, 053802 (2010).
- [28] M. Marthaler, Y. Utsumi, D. S. Golubev, A. Shnirman, and G. Schön, Lasing without inversion in circuit quantum electrodynamics, *Physical Review Letters* **107**, 093901 (2011).
- [29] W. Z. Jia, L. F. Wei, and Z. D. Wang, Tunable one-dimensional microwave emissions from cyclic-transition three-level artificial atoms, *Phys. Rev. A*

- 83**, 023811 (2011).
- [30] G. Oelsner, P. Macha, O. Astafiev, E. Il'ichev, M. Grajcar, U. Hübner, B. Ivanov, P. Neilinger, and H.-G. Meyer, Dressed-state amplification by a single superconducting qubit, *Physical review letters* **110**, 053602 (2013).
- [31] S. Ashhab, J. Johansson, A. Zagorin, and F. Nori, Single-artificial-atom lasing using a voltage-biased superconducting charge qubit, *New Journal of Physics* **11**, 023030 (2009).
- [32] F. Yan, P. Krantz, Y. Sung, M. Kjaergaard, D. L. Campbell, T. P. Orlando, S. Gustavsson, and W. D. Oliver, Tunable coupling scheme for implementing high-fidelity two-qubit gates, *Physical Review Applied* **10**, 054062 (2018).
- [33] Y. Sung, L. Ding, J. Braumüller, A. Vepsäläinen, B. Kannan, M. Kjaergaard, A. Greene, G. O. Samach, C. McNally, D. Kim, A. Melville, B. M. Niedzielski, M. E. Schwartz, J. L. Yoder, T. P. Orlando, S. Gustavsson, and W. D. Oliver, Realization of high-fidelity  $cz$  and  $zz$ -free  $i$ swap gates with a tunable coupler, *Phys. Rev. X* **11**, 021058 (2021).
- [34] W. Cai, Y. Ma, W. Wang, C.-L. Zou, and L. Sun, Bosonic quantum error correction codes in superconducting quantum circuits, *Fundamental Research* **1**, 50 (2021).
- [35] N. Ofek, A. Petrenko, R. Heeres, P. Reinhold, Z. Leghtas, B. Vlastakis, Y. Liu, L. Frunzio, S. Girvin, L. Jiang, *et al.*, Extending the lifetime of a quantum bit with error correction in superconducting circuits, *Nature* **536**, 441 (2016).
- [36] V. Sivak, A. Eickbusch, B. Royer, S. Singh, I. Tsioutsios, S. Ganjam, A. Miano, B. Brock, A. Ding, L. Frunzio, *et al.*, Real-time quantum error correction beyond break-even, *Nature* **616**, 50 (2023).
- [37] M. Gu, C. Weedbrook, N. C. Menicucci, T. C. Ralph, and P. van Loock, Quantum computing with continuous-variable clusters, *Physical Review A* **79**, 062318 (2009).
- [38] K. Marshall, C. S. Jacobsen, C. Schäfermeier, T. Gehring, C. Weedbrook, and U. L. Andersen, Continuous-variable quantum computing on encrypted data, *Nature communications* **7**, 13795 (2016).
- [39] G. R. Fowles, *Introduction to modern optics* (Courier Corporation, 1989).
- [40] J.-Q. You and F. Nori, Atomic physics and quantum optics using superconducting circuits, *Nature* **474**, 589 (2011).
- [41] X. Gu, A. F. Kockum, A. Miranowicz, Y.-x. Liu, and F. Nori, Microwave photonics with superconducting quantum circuits, *Physics Reports* **718**, 1 (2017).
- [42] M. Cassidy, A. Bruno, S. Rubbert, M. Irfan, J. Kamhuber, R. Schouten, A. Akhmerov, and L. Kouwenhoven, Demonstration of an ac josephson junction laser, *Science* **355**, 939 (2017).
- [43] G. Oelsner and E. Il'ichev, Lasing in circuit quantum electrodynamics, in *Functional Nanostructures and Metamaterials for Superconducting Spintronics: From Superconducting Qubits to Self-Organized Nanostructures*, edited by A. Sidorenko (Springer International Publishing, Cham, 2018) pp. 175–194.
- [44] J. Q. You, X. Hu, S. Ashhab, and F. Nori, Low-decoherence flux qubit, *Phys. Rev. B* **75**, 140515 (2007).
- [45] J. You, Y.-x. Liu, C. Sun, and F. Nori, Persistent single-photon production by tunable on-chip micromaser with a superconducting quantum circuit, *Physical Review B* **75**, 104516 (2007).
- [46] Z. Peng, S. De Graaf, J. Tsai, and O. Astafiev, Tuneable on-demand single-photon source in the microwave range, *Nature communications* **7**, 12588 (2016).
- [47] J. Joo, J. Bourassa, A. Blais, and B. C. Sanders, Electromagnetically induced transparency with amplification in superconducting circuits, *Phys. Rev. Lett.* **105**, 073601 (2010).
- [48] A. Blais, A. L. Grimsmo, S. M. Girvin, and A. Wallraff, Circuit quantum electrodynamics, *Reviews of Modern Physics* **93**, 025005 (2021).
- [49] C. Lang, D. Bozyigit, C. Eichler, L. Steffen, J. Fink, A. Abdumalikov Jr, M. Baur, S. Filipp, M. P. Da Silva, A. Blais, *et al.*, Observation of resonant photon blockade at microwave frequencies using correlation function measurements, *Physical review letters* **106**, 243601 (2011).
- [50] A. Sokolova, G. Fedorov, E. Il'ichev, and O. Astafiev, Single-atom maser with an engineered circuit for population inversion, *Physical Review A* **103**, 013718 (2021).
- [51] W. M. Itano, D. J. Heinzen, J. J. Bollinger, and D. J. Wineland, Quantum zeno effect, *Physical Review A* **41**, 2295 (1990).
- [52] F. De Jong, R. Spreeuw, and H. v. L. van den Heuvel, Quantum zeno effect and v-scheme lasing without inversion, *Physical Review A* **55**, 3918 (1997).
- [53] J. R. Johansson, P. D. Nation, and F. Nori, Qutip: An open-source python framework for the dynamics of open quantum systems, *Computer Physics Communications* **183**, 1760 (2012).
- [54] P. Krantz, M. Kjaergaard, F. Yan, T. P. Orlando, S. Gustavsson, and W. D. Oliver, A quantum engineer's guide to superconducting qubits, *Applied physics reviews* **6** (2019).
- [55] H. G. Ahmad, V. Brosco, A. Miano, L. Di Palma, M. Arzeo, D. Montemurro, P. Lucignano, G. P. Pepe, F. Tafuri, R. Fazio, and D. Massarotti, Hybrid ferromagnetic transmon qubit: Circuit design, feasibility, and detection protocols for magnetic fluctuations, *Phys. Rev. B* **105**, 214522 (2022).
- [56] R. Naik, N. Leung, S. Chakram, P. Groszkowski, Y. Lu, N. Earnest, D. McKay, J. Koch, and D. I. Schuster, Random access quantum information processors using multimode circuit quantum electrodynamics, *Nature communications* **8**, 1904 (2017).
- [57] W. Wang, Y. Wu, Y. Ma, W. Cai, L. Hu, X. Mu,

- Y. Xu, Z.-J. Chen, H. Wang, Y. Song, *et al.*, Heisenberg-limited single-mode quantum metrology in a superconducting circuit, *Nature communications* **10**, 4382 (2019).
- [58] A. Eickbusch, V. Sivak, A. Z. Ding, S. S. Elder, S. R. Jha, J. Venkatraman, B. Royer, S. M. Girvin, R. J. Schoelkopf, and M. H. Devoret, Fast universal control of an oscillator with weak dispersive coupling to a qubit, *Nature Physics* **18**, 1464 (2022).
- [59] L. Hu, Y.-C. Ma, Y. Xu, W.-T. Wang, Y.-W. Ma, K. Liu, H.-Y. Wang, Y.-P. Song, M.-H. Yung, and L.-Y. Sun, Simulation of molecular spectroscopy with circuit quantum electrodynamics, *Science bulletin* **63**, 293 (2018).